Research Article | Vol. 33, No. 21 / 20 Oct 2025 / Optics Express 44042
Optics EXPRESS

Tunable comb operation in terahertz quantum cascade ring lasers

MICHAEL JAIDL,[1,2,*,†] DOMINIK THEINER,[1,2,†] FLORIAN PILAT,[3] AARON M. ANDREWS,[2,3] RAHUL YADAV,[4] GOTTFRIED STRASSER,[2,3] BENEDIKT SCHWARZ,[2,3] SASCHA PREU,[4] JURAJ DARMO,[1,2] AND KARL UNTERRAINER[1,2]

[1]*Photonics Institute, TU Wien, Gusshausstrasse 27-29, 1040 Vienna, Austria*
[2]*Centre for Micro- and Nanostructures, TU Wien, Gusshausstrasse 25a, 1040 Vienna, Austria*
[3]*Institute of Solid-State Electronics, TU Wien, Gusshausstrasse 25a, 1040 Vienna, Austria*
[4]*Department of Electrical Engineering and Information Technology, TU Darmstadt, 64283 Darmstadt, Germany*
[†]These authors contributed equally to this work.
[*]*michael.jaidl@tuwien.ac.at*

Abstract: We demonstrate a versatile and compact approach to generate and control terahertz frequency combs by applying radio frequency modulation to a ring-shaped quantum cascade laser. By harmonically driving the device well above threshold, we induce the formation of phase-coherent sidebands with tunable spacing across a broad radio frequency range (1.5–14.5 GHz), independent of the laser's cavity modes. The RF generated comb exhibits narrow beat notes with linewidths down to 3.5 Hz and a linear phase profile, as verified by optical beat note analysis, indicating the important role of the phase modulation. Unlike classical phase modulation, we observe a simultaneous increase in total terahertz output power and driving current, reflecting an enhanced laser efficiency and photon-assisted transport. The presented approach enables flexible manipulation of frequency grids and spectral power distribution in both single-mode and multimode regimes, including subharmonic injection locking for spectral broadening. Our results highlight the potential of radio frequency-modulated quantum cascade lasers as customizable, high-efficiency terahertz comb sources for spectroscopy, sensing, and communication applications.

Published by Optica Publishing Group under the terms of the Creative Commons Attribution 4.0 License. Further distribution of this work must maintain attribution to the author(s) and the published article's title, journal citation, and DOI.

1. Introduction

Since their introduction, optical frequency combs [1] have become indispensable tools for linking optical frequencies to radio frequencies with exceptional precision. Originally developed in the context of femtosecond mode-locked lasers, frequency combs were instrumental in the development of optical atomic clocks. Over the past two decades, the scope of optical frequency combs has expanded dramatically beyond fundamental physics. They are now integral to applications ranging from high-resolution molecular spectroscopy and distance metrology to astronomical spectrograph calibration and coherent optical communications. Recent advances have pushed the development of compact, chip-scale comb generators using nonlinear microresonators, electro-optic modulation, and quantum cascade lasers, enabling broader accessibility and integration into practical systems.

In the terahertz (THz) regime, different approaches can be used to generate frequency combs. One of the most established techniques involves the use of femtosecond mode-locked lasers to generate THz radiation via photo-conductive antennas or optical rectification in nonlinear crystals [2]. However, this approach suffers from weak output powers and often bulky and expensive

#545805 https://doi.org/10.1364/OE.545805
Journal © 2025 Received 21 Oct 2024; revised 25 Sep 2025; accepted 25 Sep 2025; published 10 Oct 2025

Optics EXPRESS

equipment. A more flexible approach in terms of frequency tunability is difference frequency mixing in a photo-conductive device [3]. By utilizing the established technique of near-infrared electro-optic combs which are converted to the THz spectral region, on demand spectra can be synthesized. Still, weak output powers and the restriction to lower THz frequencies due to the decreasing conversion efficiency are limiting the performance. THz quantum cascade lasers (QCLs) [4] come with a broad design parameter space, high output power and compactness. In recent years, frequency comb formation in THz QCLs has been reported [5,6]. Due to strong optical non-linearities resulting from the intersubband transition in these devices, phase locking of the intracavity modes is achieved by four-wave mixing in the gain medium. These non-linearities are even stronger in ring-shaped cavities compared to commonly used ridge-type waveguides due to the enhanced mode confinement. Therefore, ring resonators provide an ideal platform for comb formation [7,8].

Radio frequency (RF) modulation of semiconductor lasers is very well studied [9,10] and has recently gained increased attention for QCLs. RF injection locking or modulation at the cavity round-trip frequency can stabilize the intermode beat note of a QCL comb. This enhances phase coherence and reduces linewidth, making the comb more useful for high-precision applications such as dual-comb spectroscopy. Strong RF injection at resonance leads to a quantum walk state, resulting in large broadening of the emitted bandwidth [11]. In dual-comb spectroscopy, two QCL combs with slightly different repetition rates are used to down-convert THz signals into the RF domain. RF modulation facilitates precise control over comb parameters, ensuring the required offset for dual-comb operation.

Usually, the modulation frequency is set close to the roundtrip frequency (or its higher harmonics resp. subharmonics) defined by the cavity [12–17]. RF modulation of THz QCLs at off-resonant modulation frequencies was studied by up-conversion of THz photons to a 1.57 μm carrier [18] which demonstrates the importance of the huge contribution of the complex intersubband susceptibility. In a very recent work [19], strong RF driving of THz QCLs resulted in the observation of pulses with tunable repetition rate. It would be attractive to combine the flexibility of the electro-optic comb formation approach [3] and the compactness with sufficient output powers of THz QCLs to obtain a flexible and powerful comb source for e.g. spectroscopic applications.

In this paper, we study RF driving of a THz QCL significantly above threshold and show that the generated sidebands can be tuned continuously by the injected modulation frequency. The comb lines are mutually coherent with a linear phase.

To study the RF modulation capability of a QCL, we adopted a ring geometry, leveraging multiple advantages: first, it adheres to the conventional QCL geometry, promoting controlled single- or multi-mode operation for the laser source; second, it enhances the potential modulation depth for the RF modulator. This increased modulation depth is attributed to the extended path length within the ring structure, allowing the electromagnetic wave to undergo multiple roundtrips before exiting the cavity, thereby experiencing intensified modulation effects; and third, ring resonators are well suited for frequency comb formation, as previous works have shown [7,8,20].

2. Results

Detailed information about the device and the experimental setup can be found in Supplement 1. In brief, the QCL is running in single-mode emission from the threshold current of 314 mA until the current level of 340 mA, where a free-running comb regime starts with an optical beatnote at 13.1 GHz and a linewidth of 339 kHz. When such a QCL is operating in the single-mode regime, we demonstrate that a harmonic RF driving generates sidebands around the single-mode center frequency of the free-running device that follow deterministically the RF driving frequency (1.5 - 14.5 GHz), yielding multiple frequency-equidistant modes, as shown in the heatmap of Fig. 1(a). In Fig. 1(b)-(d) we show three spectra at different modulation frequencies which are far off the

Optics EXPRESS

roundtrip frequency of the cavity. Note, that the spectral resolution of the FTIR in use is 2.7 GHz. Notably, the RF modulation is frequency-wise not restricted by the cavity modes and can be detuned continuously throughout the whole RF range. A modulation close to the roundtrip frequency (or its subharmonics) rather leads to a broadening of the emission spectrum.

For further characterization of our multimode emission spectrum we perform optical beat note measurements using a zero-bias TeraFET [21]. The direct measurement of the common beat note spectrum indicates a fixed phase relation between the modes. Figure 1(e) shows clearly that the modes generate a single beating signal with a signal-to-noise ratio up to 40 dB in the RF spectrum (and its higher harmonics). A Gaussian fit of the data reveals a linewidth of 3.5 Hz mainly limited by the noise of the RF equipment, which indicates the frequency comb nature of our multimode emission spectrum.

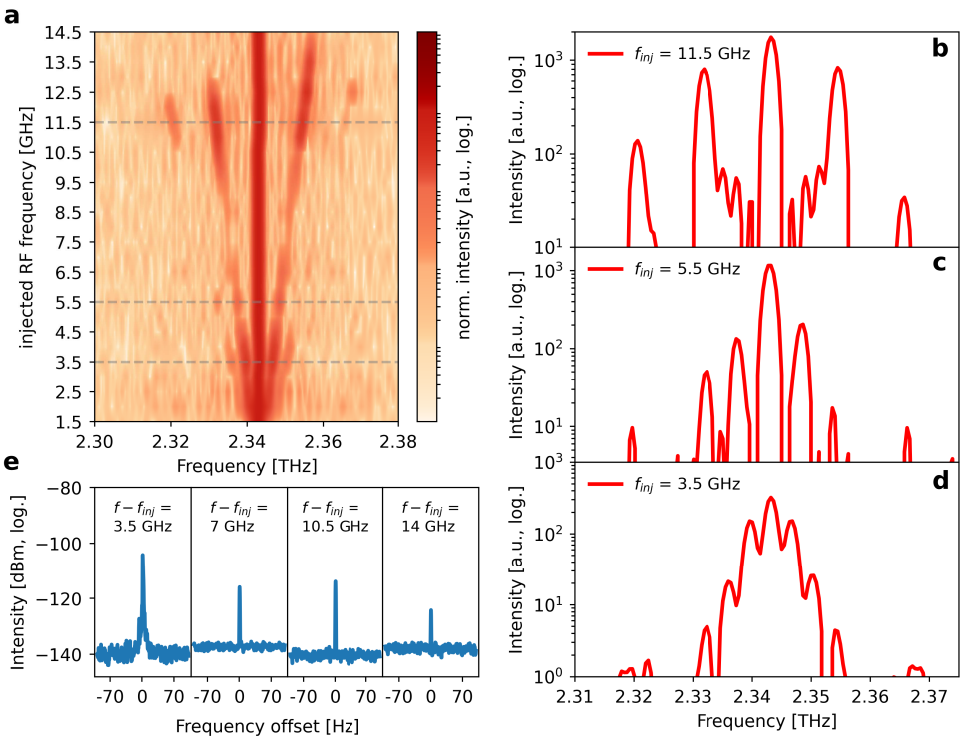

Fig. 1. RF modulation of the ring QCL operated in the single-mode regime. (a) Intensity map of the spectral distribution over an injected RF from 1.5 to 14.5 GHz with a nominal power of 18.9 dBm. The dashed gray line indicates the positions of the spectra shown in (b)-(d) at modulation frequencies of 11.5 GHz, 5.5 GHz and 3.5 GHz. The spectral resolution of the used FTIR is 2.7 GHz. (e) Optical beat note spectrum of the modes shown in (d). The spectrum generated by RF modulation forms a frequency comb, hence, all mode pairs create a beating signal at their frequency spacing (i.e., a multiple of the driving RF frequency) with a linewidth of 3.5 Hz mainly limited by the RF equipment.

At a constant RF frequency and an increasing RF power, the sideband spectrum becomes increasingly prominent (Fig. 2(a)), which was also observed in Ref. [11]. In the classical phase modulation picture, the power of a single-mode laser is redistributed to its newly generated sidebands, resulting in a decrease in the carrier signal amplitude, while the total number of photons remains constant. Remarkably, we note a significant departure from that model in our system, as the central mode remains at a constant power level even as the sidebands grow stronger (spectra not normalized). This leads to an increase in the overall photon count as shown in

Optics EXPRESS

Fig. 2(b), which is also reflected in the rising driving current of the QCL, since the additional photon flux increases the photon-assisted transport through the quantum-well structure [22]. The increase in current by 1.0‰ and the applied RF power, constituting <2% of the total power supplied by the DC source (5 W), cannot explain the observed 100% rise in overall output power. If one compares the output power values for the current values for the unmodulated and maximum modulated case in the unmodulated LIV (see Supplement 1 Fig. S2), the increase of the output power is about 38%. However, we observe a doubled output power for the maximum modulated case compared to the unmodulated one. This indicates a substantial improvement in the extraction efficiency (almost double) of the energy stored in the upper laser levels of the QCL. The RF modulation of our QCL ensures better utilization of the entire laser gain, surpassing the efficiency achieved for gain-clamped free-running single-mode driving conditions. A significant non-homogeneous broadening of the QCL gain [23] or spatial hole burning could limit the gain competition among the newly generated modes. The interferogram, shown in Fig. 2(c) for the spectrum generated with an RF power of 18.9 dBm, verifies that the coherence of the frequency comb remains even under high-power driving conditions.

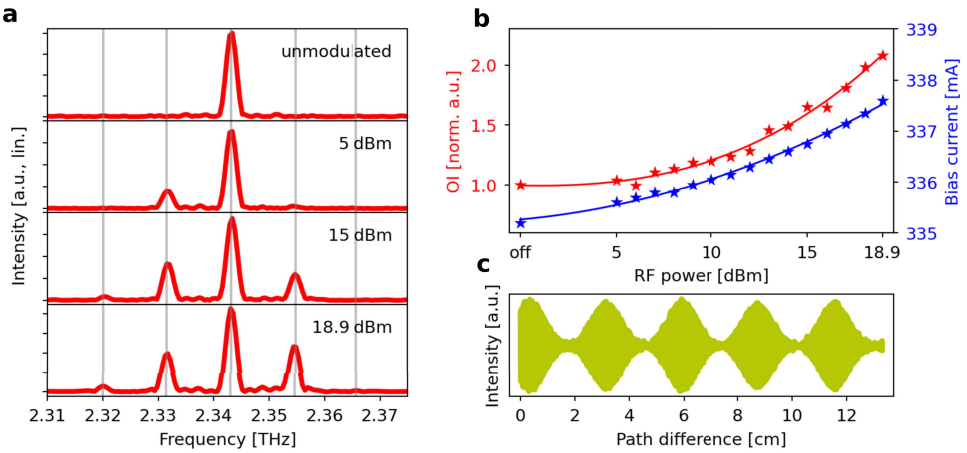

Fig. 2. Power sweep of the injected RF signal at 11.6 GHz. (a) The QCL is operated in constant voltage operation at a fixed bias voltage point. Due to an increasing modulation depth with rising RF power, sidebands proliferate, and their amplitudes are rising, due to the raised distribution of the central line power. The gray lines indicate the mode spacing at the injected frequency of 11.6 GHz. (b) The red curve (left y-axis) shows the overall emission intensity (OI) (as calculated from the area under the curve) for the spectra at different injected power levels (spectra not normalized). Due to the inherent gain of the QCL, the central mode is amplified and stays at the same intensity level despite the redistribution of its power to the generated sidebands. This effect is also manifested in an increase in the driving current (blue curve, right y-axis). In this way, the gain is utilized more efficiently than in the free-running operation and the output power is doubled comparing the unmodulated and maximal modulated case. (c) Interferogram of the RF modulated spectrum at an injected RF power of 18.9 dBm (bottom of (a)), showing the strong coherence of the generated frequency comb.

In order to verify that the output of the QCL is indeed a frequency comb, a SWIFTS measurement [5] is performed. In this way, it is possible to extract the phase difference between adjacent modes and to reconstruct the intensity profile in the time domain. Figure 3(a) shows the intensity (measured with a slow DTGS detector) and SWIFTS (measured with a fast Schottky diode detector) spectra together with the phase difference between the modes for the device operated in the single-mode regime and RF modulated with a frequency of 12.4 GHz and a

Optics EXPRESS

nominal power of 23 dBm. The phase difference shows a linear behavior. This indicates that phase modulation is dominating amplitude modulation in our system. For dominant amplitude modulation such as active mode-locking reported in [19] one would expect a constant phase of the modes. In Fig. 3(b) the reconstructed intensity profile in the time domain is shown. It can be seen that the temporal intensity varies which causes an observable beat note signal. In contrast to amplitude modulated spectra, where short pulses are expected, the reconstruction of the time profile exhibits intensity variations but no short pulses.

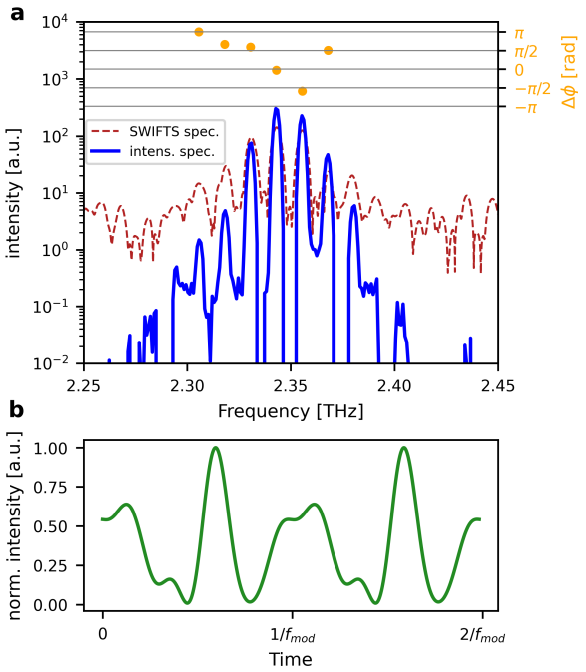

Fig. 3. SWIFT spectroscopy measurement. The measurement is performed with the ring laser operating in the single-mode regime and modulated at 12.4 GHz with a nominal power of 23 dBm. (a) Intensity spectrum (blue, measured with a slow DTGS detector) and SWIFTS spectrum (red, measured with a fast Schottky diode detector). The phase difference between the modes exhibits a linear behavior, indicating dominant phase modulation rather to amplitude modulation. (b) Reconstructed time profile showing intensity variations.

To understand the strong phase modulation we have to look at the susceptibility of the laser transition which determines the gain by the imaginary part and the induced refractive index change by its real part. For simple two-level systems, the real part of the susceptibility is anti-symmetric and vanishes at resonance. However, many laser systems have very complex susceptibilities originating from the involved quantum levels resulting in an asymmetry and a non-vanishing real part at resonance. In interband semiconductor lasers, also the plasma response of free carriers contributes significantly to the phase change which makes their modulation quite complicated due to different dynamics. The situation is different in QCLs, where the gain is connected to the population difference between the quantized levels and not to the carrier concentration. The optical intersubband matrix element is large and several applications of the giant susceptibility associated with intersubband transitions have been proposed [24]. The real part of the intersubband susceptibility especially in THz devices can be quite asymmetric due to contributions from the Bloch gain [23,25]. This causes a large linewidth enhancement factor which has been found to be decisive for frequency comb formation [26].

Optics EXPRESS

We model the complex susceptibility of a QCL adding a Bloch contribution to the two-level oscillator term following Opačak et al. [25]:

$$\chi_{ul}(\omega) = \frac{\mu_{ul}^2}{\varepsilon_0 \hbar} N \frac{(f_u - f_l)}{\omega_{ul} - \omega - i\gamma_{ul}}(1 + ib) \tag{1}$$

with the electron density N, the relative population difference $f_u - f_l$, the dipole matrix element of the lasing transition μ_{ul}^2, the transition frequency ω_{ul}, the frequency ω, and the transition linewidth γ_{ul}. The b-parameter is known as the linewidth enhancement factor which in the case of QCLs also includes the contribution from the Bloch gain [25].

A quick analysis of Eq. (1) yields the key fact that the real part of susceptibility at resonance is non-zero and is even larger than the imaginary part of the susceptibility by the b-parameter. Thus, RF modulation of a QCL indeed leads to a substantial modulation of the real part of the susceptibility. Therefore, we expect significant phase modulation in these devices. Furthermore, the gain dynamics of QCL active regions is very fast allowing very high modulation bandwidths [27,28]. Due to an absence of a plasma response of free carriers, the phase change is directly connected to the intersubband susceptibility and determined by its dynamics. We have simulated the RF response (see Supplement 1 Fig. S4) and obtain sideband generation entirely due to phase modulation. Since the bandwidth of the detector is limited, a filter function is applied to the simulated signal. The resulting phase modulation signal features an intensity time profile comparable to the reconstructed time profile from the SWIFTS measurement.

By changing the operation point of the QCL via the driving current, the QCL can be tuned from single-mode to comb operation, as depicted in the first panel of Fig. 4(a). This represents a free-running frequency comb [7] (see Supplement 1 Fig. S2). Applying an additional RF signal to the QCL while operating in the free-running comb regime generates sidebands on several of the free-running modes, leading to multiple mode groups in the spectrum, as shown in the further panels of Fig. 4(a). Additionally, the RF modulation leads to a frequency offset of the mode groups compared to the free running-spectrum (offset to the gray lines) and changes the intensity distribution between the original free-running modes. Notably, in the resulting spectra, two distinct frequency grids emerge: the inherent free-running mode spacing of 13 GHz and the grid imposed by the applied modulation frequency. Therefore, adjacent mode groups exhibit a frequency spacing that reflects the difference between these grids, as exemplified in Fig. 4(b), where a 200 MHz offset is observed between two neighboring mode groups, which is evidently better seen in the beat note spectrum due to the resolution limit of 2.7 GHz of the utilized Fourier-transform infrared (FTIR) spectrometer. It has to be noted that this offset frequency is determined by the offset of the modulation frequency (respectively multiples of it) and the free-running comb spacing. The RF spectrum consists of the beating within the mode groups, defined by the modulation frequency (and its higher harmonics), which are again characterized by a Hz level linewidth (highlighted in orange), and secondly by the free-running comb beat note at 13 GHz with a linewidth of 39 MHz (highlighted in green). In addition, several mixing frequencies between them can be observed due to the non-linear laser medium in which all the modes arise which exhibit a broad linewidth as well (highlighted in green).

When the RF driving frequency reaches a subharmonic resonance of the ring cavity (e.g. a subharmonic of the free-running comb spacing), the entire system resonates, yielding a spectral broadening, as evidenced by the spectrum generated with a driving frequency of 3.47 GHz. This resonant scenario can be further interpreted as subharmonic injection locking of the free-running QCL comb, underscoring the intricate dynamics underlying the RF modulated multimode operation and verified by the substantial narrowing of the comb beat note (see Fig. 4(c)) compared to the free-running operation.

Optics EXPRESS

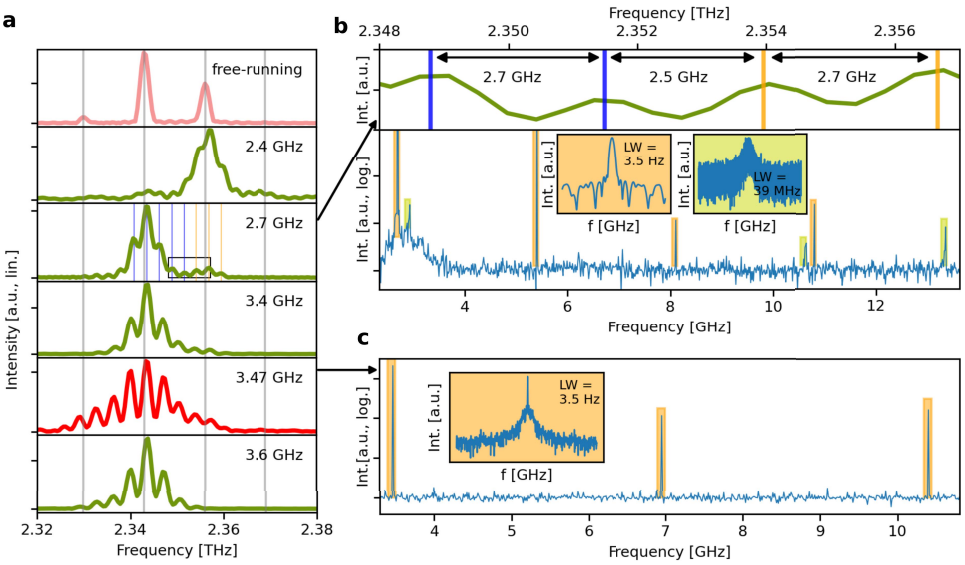

Fig. 4. RF modulation of the ring QCL operated in the multimode regime at a driving current of 367 mA. (a) Spectral evolution over different modulation frequencies. In non-resonant cases (e.g., if the modulation frequency does not match a subharmonic of the roundtrip frequency), the free-running modes are modulated individually, leading to an offset frequency between the mode groups. (b) An example for a modulation frequency of 2.7 GHz. The upper part displays a zoom-in of the neighboring mode groups with an offset frequency of 200 MHz. This offset becomes more evident in the beat note spectrum (lower part of (b)). Modes which are generated by the RF modulation create a narrow Hz-level beating at the modulation frequency and its higher harmonics (orange). However, the free-running modes beat at the roundtrip frequency with a comparatively broad linewidth and furthermore produce beatings with the generated modes (green). If the modulation frequency corresponds to a subharmonic of the roundtrip frequency, the frequency comb is fully locked and no offset frequency between individual mode groups appears. As a result, mode pairs create beat note signals at the modulation frequency and its higher harmonics only (shown in (c)) for a modulation frequency of 3.47 GHz) and the free-running beat note is substantially narrowed by the locking mechanism.

3. Conclusion

Through the utilization of an all-electronic frequency flexible control mechanism we showcase the ability to manipulate and tailor the emission spectrum of a QCL. Specifically, the frequency spacing and power distribution among the spectral lines are directly governed by the modulation parameters: RF frequency and RF input power. The phase differences and the reconstructed time profile obtained by the SWIFTS measurement indicate a significant phase modulation. Since we are working with an intersubband transition amplifying medium, contributions by amplitude modulation cannot be excluded. Our modulation scheme shows that phase modulation allows the generation of a comb from a THz QCL single line at almost maximum intensity by applying only moderate RF power. This allows for precise control over the line spacing, the number of lines, and their spectral power distribution, enabling seamless switching between different spectral configurations, virtually instantaneously since the phase change dynamics is directly governed by the intersubband dynamics. The current parametric space for the spectral shaping can easily be widened by adopting more advanced modulation schemes than simple harmonic driving (e.g., a chirped pulse form) [29] to generate rich comb spectra. A proper RF design for

Optics EXPRESS

enhanced efficiency of RF power injection, via an impedance matching between the source and the QCL device, will further increase the reachable modulation depth and reduce the required RF powers. Our findings pave the way for compact and efficient devices capable of simultaneous laser emission and phase modulation. It allows the generation of customized frequency combs not restricted by the cavity modes and amplified by the spectral gain of the underlying QCL, with promising implications for diverse applications in spectroscopy, communications, and optical data processing. Especially its application in the terahertz domain brings great advantages, since many molecules relevant for medical analysis and environmental monitoring exhibit rotational modes in this frequency region [30], accessible by a spectrally flexible QCL device.

Funding. Austrian Science Fund (TeraLearn P35932-N, Everest I 5772); Hochschuljubiläumsstiftung der Stadt Wien (H-864343/2022); Österreichische Forschungsförderungsgesellschaft (Green Sensing 883941); European Office of Aerospace Research and Development (FA8655-22-1-7170, FA8655-23-1-7070).

Acknowledgments. The authors acknowledge financial support from the Austrian Science Fund FWF (TeraLearn P35932-N, Everest I 5772) D.T. acknowledges funding through the Hochschuljubiläumsfonds der Stadt Wien. A.M.A. acknowledges the support of the European Office of Aerospace Research and Development/ Air Force Office of Scientific Research (EOARD/AFOSR No. FA8655-22-1-7170 and FA8655-23-1-7070), and the Austrian Research Promotion Agency (FFG) Project Green Sensing (No. 883941).

Disclosures. The authors declare no conflicts of interest.

Data availability. Data underlying the results presented in this paper are not publicly available at this time but may be obtained from the authors upon reasonable request.

Supplemental document. See Supplement 1 for supporting content.

References

1. T. Udem, R. Holzwarth, and T. W. Hänsch, "Optical frequency metrology," Nature **416**(6877), 233–237 (2002).
2. M. Tonouchi, "Cutting-edge terahertz technology," Nat. Photonics **1**(2), 97–105 (2007).
3. D. Theiner, B. Limbacher, M. Jaidl, *et al.*, "Flexible terahertz opto-electronic frequency comb light source tunable over 3.5 THz," Opt. Lett. **46**(22), 5715–5718 (2021).
4. R. Köhler, A. Tredicucci, F. Beltram, *et al.*, "Terahertz semiconductor-heterostructure laser," Nature **417**(6885), 156–159 (2002).
5. D. Burghoff, T.-Y. Kao, N. Han, *et al.*, "Terahertz laser frequency combs," Nat. Photonics **8**(6), 462–467 (2014).
6. J. Faist, G. Villares, G. Scalari, *et al.*, "Quantum Cascade Laser Frequency Combs," Nanophotonics **5**(2), 272–291 (2016).
7. M. Jaidl, N. Opacak, M. A. Kainz, *et al.*, "Comb operation in terahertz quantum cascade ring lasers," Optica **8**(6), 780–787 (2021).
8. M. Jaidl, N. Opacak, M. A. Kainz, *et al.*, "Silicon integrated terahertz quantum cascade ring laser frequency comb," Appl. Phys. Lett. **120**(9), 091106 (2022).
9. S. E. Harris, "Stabilization and Modulation of Laser Oscillators by Internal Time-Varying Perturbation," Appl. Opt. **5**(10), 1639–1651 (1966).
10. R. Tucker and I. Kaminow, "High-frequency characteristics of directly modulated InGaAsP ridge waveguide and buried heterostructure lasers," J. Lightwave Technol. **2**(4), 385–393 (1984).
11. I. Heckelmann, M. Bertrand, A. Dikopoltsev, *et al.*, "Quantum walk comb in a fast gain laser," Science **382**(6669), 434–438 (2023).
12. P. Gellie, S. Barbieri, J.-F. Lampin, *et al.*, "Injection-locking of terahertz quantum cascade lasers up to 35GHz using RF amplitude modulation," Opt. Express **18**(20), 20799 (2010).
13. A. D. Gaspare, L. Viti, H. E. Beere, *et al.*, "Homogeneous quantum cascade lasers operating as terahertz frequency combs over their entire operational regime," Nanophotonics **10**(1), 181–186 (2020).
14. M. S. Vitiello and P. De Natale, "Terahertz Quantum Cascade Lasers as Enabling Quantum Technology," Adv. Quantum Technol. **5**(1), 2100082 (2022).
15. S. Barbieri, M. Ravaro, P. Gellie, *et al.*, "Coherent sampling of active mode-locked terahertz quantum cascade lasers and frequency synthesis," Nat. Photonics **5**(5), 306–313 (2011).
16. F. Wang, V. Pistore, M. Riesch, *et al.*, "Ultrafast response of harmonic modelocked THz lasers," Light: Sci. Appl. **9**(1), 51 (2020).
17. N. Henry, D. Burghoff, Q. Hu, *et al.*, "Temporal characteristics of quantum cascade laser frequency modulated combs in long wave infrared and THz regions," Opt. Express **26**(11), 14201–14212 (2018).
18. S. Barbieri, W. Maineult, S. S. Dhillon, *et al.*, "13 GHz direct modulation of terahertz quantum cascade lasers," Appl. Phys. Lett. **91**(14), 143510 (2007).
19. U. Senica, M. A. Schreiber, P. Micheletti, *et al.*, "Continuously tunable coherent pulse generation in semiconductor lasers," arXiv (2024).

Optics EXPRESS

20. P. Micheletti, U. Senica, A. Forrer, *et al.*, "Terahertz optical solitons from dispersion-compensated antenna-coupled planarized ring quantum cascade lasers," Sci. Adv. **9**(24), eadf9426 (2023).
21. S. Regensburger, A. k. Mukherjee, S. Schönhuber, *et al.*, "Broadband Terahertz Detection With Zero-Bias Field-Effect Transistors Between 100 GHz and 11.8 THz With a Noise Equivalent Power of 250 pW/$\sqrt{Hz}$ at 0.6 THz," IEEE Trans. Terahertz Sci. Technol. **8**(4), 465–471 (2018).
22. A. Forrer, M. Franckié, D. Stark, *et al.*, "Photon-Driven Broadband Emission and Frequency Comb RF Injection Locking in THz Quantum Cascade Lasers," ACS Photonics **7**(3), 784–791 (2020).
23. H. Willenberg, G. H. Döhler, and J. Faist, "Intersubband gain in a Bloch oscillator and quantum cascade laser," Phys. Rev. B **67**(8), 085315 (2003).
24. J.-Y. Duboz, P. Bois, and E. Rosencher, "Intersubband Transitions in Quantum Wells," in *Confined Electrons and Photons: New Physics and Applications*, E. Burstein and C. Weisbuch, eds. (Springer US, 1995), pp. 249–268.
25. N. Opacak, S. D. Cin, J. Hillbrand, *et al.*, "Frequency Comb Generation by Bloch Gain Induced Giant Kerr Nonlinearity," Phys. Rev. Lett. **127**(9), 093902 (2021).
26. M. Piccardo, B. Schwarz, D. Kazakov, *et al.*, "Frequency combs induced by phase turbulence," Nature **582**(7812), 360–364 (2020).
27. C. Y. Wang, L. Kuznetsova, V. M. Gkortsas, *et al.*, "Mode-locked pulses from mid-infrared Quantum Cascade Lasers," Opt. Express **17**(15), 12929–12943 (2009).
28. C. G. Derntl, G. Scalari, D. Bachmann, *et al.*, "Gain dynamics in a heterogeneous terahertz quantum cascade laser," Appl. Phys. Lett. **113**(18), 181102 (2018).
29. D. A. Long, A. J. Fleisher, D. F. Plusquellic, *et al.*, "Multiplexed sub-Doppler spectroscopy with an optical frequency comb," Phys. Rev. A **94**(6), 061801 (2016).
30. I. E. Gordon, L. S. Rothman, R. J. Hargreaves, *et al.*, "The HITRAN2020 molecular spectroscopic database," J. Quant. Spectrosc. Radiat. Transf. **277**, 107949 (2022).

136.130.242.41 2025-10-13 07:26 C